Mathematical Models for Simultaneous Particle Dissolution and Nucleation during Heat Treatment of Aluminium Alloys

INTERIM THESIS

F.J. de Zwaan

January 6, 2006

Thesis Committee
Dr. C. Liu (Corus Research, Development & Technology)
Ir. H.F.M. Corstens (Delft University of Technology)
Prof.dr.ir. P. Wesseling (Delft University of Technology)
Dr.ir. C. Vuik (Delft University of Technology)
Dr.ir. F.J. Vermolen (Delft University of Technology)

Contents

Chapter 1

Introduction

1.1 About Corus

Corus is a leading international metal company which combines world renowned expertise with local service. The headquarters are in London, with four divisions and operations worldwide. The company has manufacturing operations in many countries, with major plants in the UK, the Netherlands, Germany, France, Norway and the USA. In addition, a network of sales offices and service centres spans the globe. The shares are listed on the London, New York and Amsterdam stock exchanges.

In 2004 Corus generated a turnover of £9.3 billion and produced 19 million tonnes of steel and delivered over 0.6 million tonnes of aluminium. At the end of December 2004 Corus had 48,300 employees.

From October 2003 Corus has been structured into four main divisions: Strip Products, Long Products, Aluminium and Distribution and Building Systems.

Corus was formed on 6th October 1999, through the merger of British Steel and Koninklijke Hoogovens.[1]

1.2 Heat treatments and homogenization

The production of aluminium is a complicated process that requires many steps before the semi-finished product is ready for use in its applications. The base material for aluminium production is bauxite. By means of the *Bayer process* a material called *alumina* can be extracted from the bauxite. Next, an electrolysis process called the *Hall-Héroult process* is used to extract so-called *primary aluminium* from the alumina[2]. This aluminium is cast into ingots for subsequent remelting or more usually into cylindrical extrusion billets or rectangular rolling slabs. Ingots are used to produce cast products like engine blocks. Extrusion billets are pushed through shape dies to give an extruded profile used, for example, in structures while rolling slabs are hot rolled and usually cold

[1] Source: www.corusgroup.com.

[2] Since the electrolysis process requires an extraordinary amount of energy (anywhere from 12.8 to 15.5 kWh/kg), aluminium can also be recycled at 5% of the cost of production from bauxite.

rolled into sheet, plate or foil used, for example, for facade panels or packaging applications.

Since these applications vary from lawn furniture to engine blocks and from food containers to armoured plating, it is obvious that the diversity in quality requirements is quite high. Therefore, constant effort is put into finding better aluminium alloy compositions and processing techniques to meet these ever-increasing demands.

The qualitative properties of aluminium depend on a number of things, but we will only focus on the local compositions of an alloy specimen. Our main tool for influencing these compositions is the *heat treatment*: a combination of heating and cooling operations timed and applied to a metal or alloy in the solid state in a manner that will produce desired mechanical properties.

One specific type of heat treatment is the so-called *homogenization process*. After casting, the ingot/billet/slab may contain precipitates and a supersaturated phase (see also paragraph 2.1.4). To relieve the material of these inhomogeneities, the material is heat treated. Several metallurgical processes can take place during this homogenization process:

- Dissolution of precipitates present as isolated particles or as segregation layers on grain boundaries.
- Precipitation of new particles due to the "surplus" of alloying elements present in the supersaturated phase.
- Shape change of precipitates that can not completely dissolve.

1.3 Problem formulation

Traditionally, finding good heat treatments for aluminium is a process of trial and error. Often, multiple experiments have to be carried out to determine the effects of a certain heat treatment. Although mathematical models can probably not eliminate the need for physical experiments, they can help reduce the number of experiments required to determine the optimal heat treatment for a certain alloy. Therefore in the past several models have been developed in order to describe the processes that take place during a heat treatment. Some of these models were able to model particle dissolution of a single precipitate inside a grain, and others modeled the kinetics of a particle size distribution function with the use of classical nucleation theory. In this study an effort is made to combine diffusion and classical nucleation theory in one mathematical model. The main questions are

- How, and to what extent does nucleation influence particle dissolution?
- Conversely, in what way does particle dissolution influence nucleation?

In this study, the subject of interest is the mathematical modelling of heat treatments of metal alloys in general, and homogenization of aluminium in particular.

1.4 Thesis outline

This study was performed to gather the basic knowledge required to solve the problem described above. In the next chapter some important materials science

topics will be discussed. Chapter 3 will summarize the mathematical laws that will be used to describe the phenomena as presented in Chapter 2. As will be shown later, the particle dissolution problem is a special one in the field of mathematics. Some of its properties will be discussed in Chapter 4. After that will we continue by describing the methods to solve the previously described problems using a digital computer in Chapter 5. In Chapter 6 some results produced by these methods will be compared to the results of the original implementations of the respective algorithms. Finally, the directions in which to proceed in the second part of the study are outlined in Chapter 7.

Chapter 2

Preliminaries in materials science

This chapter contains a condensed view of the concepts and principles in thermodynamics and kinetics necessary for the creation of the homogenization model. Most of the material found in this chapter is explained in Porter and Easterling [1981] in much more detail. This book is recommended to everyone interested in the subject of phase transformations in metals. The work of Callister [1999] serves as a good general introduction to materials science.

2.1 Basic concepts in thermodynamics

2.1.1 Phase transformations

To understand the concepts of phase transformations we need to know what a phase is. According to Callister [1999], a phase is "a homogeneous portion of a system that has uniform physical and chemical characteristics". If more than one phase is present in a system, each one will have its own distinct properties and a boundary separating the phases will exist across which there will be a discontinuous and abrupt change in physical and/or chemical characteristics. This boundary is commonly referred to as the interface and in the case of a phase transformation it is allowed to move.

2.1.2 Equilibrium

The reason a phase transformation occurs is because the initial state of the material under investigation is unstable. The stability of a system is determined by its Gibbs free energy. The Gibbs free energy of a system is defined as

$$G = H - TS,$$

with

$$H = E + PV,$$

in which E is the internal energy of the system, P is the pressure, V is the volume, T the temperature in Kelvin, and S is the entropy of the system. The

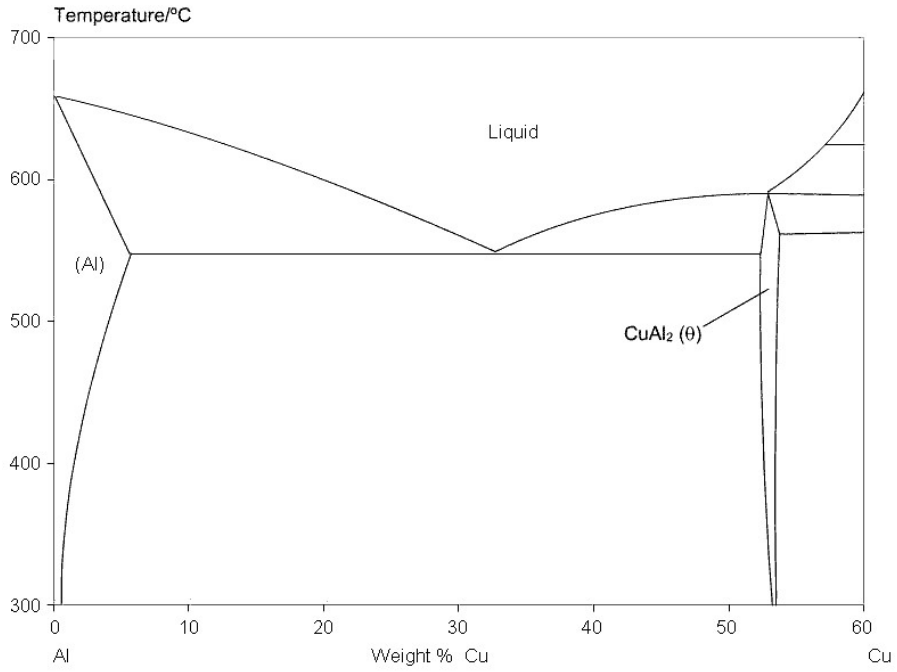

Figure 2.1: Aluminium-Copper phase diagram.

internal energy is the sum of the total kinetic and potential energy present in the system. Entropy is a measure of the randomness of the system.

A system is in equilibrium if it is in its most stable state. The laws of thermodynamics dictate that at constant temperature and pressure a closed system is in *stable equilibrium* if it has the minimum amount of Gibbs free energy, i.e. the Gibbs free energy has attained a global minimum. We say that a system is in *metastable equilibrium* if the Gibbs free energy is at a local minimum. In theory all metastable systems will transform into a stable state given enough time. A system that is neither stable nor metastable is said to be *unstable*. Unstable states are only realized for very short periods of time when the system is reorganizing itself to one of the stable or metastable states. Phase transformations occur because the system always tries to attain the lowest energy state. Therefore any transformation that decreases the Gibbs free energy is allowed. Note that through the use of only thermodynamics no claims can be made about the time it takes for metastable states to transform into stable states.

2.1.3 Phase diagrams

The relations between temperature, alloy composition and phase are most easily represented as a phase diagram. An example of such a phase diagram is shown in Figure 2.1. On the horizontal axes we see composition, on the vertical axes temperature. A lot of information can be deduced from these diagrams. We can deduce which phases are present, the composition of the phases and the phase

amounts. See Callister [1999] for more information.

2.1.4 Metastable solutions

The rules described above are valid only for situations in which thermodynamic equilibrium is maintained at all times. In practice this will rarely be the case. If we cool an alloy very rapidly we will see that there will not be enough time for the atoms to reorganize themselves to Cu-rich precipitates. The lower temperature will reduce the rate at which the elements restructure themselves by several orders of magnitude. In practice this means that the alloy is essentially frozen into a state of supersaturation; the material consists of only an Al-rich phase that contains more copper than could be dissolved in thermodynamic equilibrium. Because of the low temperature this state can be maintained almost indefinitely. This dramatic decrease in activity in the material can be explained by the temperature dependence of the diffusion coefficient (see also Section 2.3).

2.2 Material structure

An aluminium specimen is not a continuous, homogeneous volume of material. In fact it consists of billions of microscopic grains (see Figure 2.2). These grains are the subject of our investigation. We assume that the compositions of neighbouring grains are close to identical and that no concentration gradients exist between these grains. Therefore we will assume that no material is exchanged between grains.

2.3 Diffusion

One of the most fundamental processes that controls the transfer of components through the system is diffusion. There are two common mechanisms by which atoms can diffuse through a solid. Which of these mechanisms actually occurs depends on the type of site occupied in the lattice.

2.3.1 Substitutional diffusion

The first mechanism involves the movement of an atom from a normal lattice position to an adjacent vacant lattice site. Because the vacancy and the atom substitute positions this mechanism is named *substitutional diffusion*. For obvious reasons it is also known as *vacancy diffusion*. It is clear that the rate at which substitutional diffusion occurs is directly related to the number of vacancies present in the material.

2.3.2 Interstitial diffusion

Interstitial diffusion occurs when the atoms of the solute are small in comparison with the atoms of the solvent. This means that solute atoms can reside in between solvent atoms, i.e. at the interstitial positions (hence the name). Since the interstitial atoms are smaller, they can travel through the lattice much

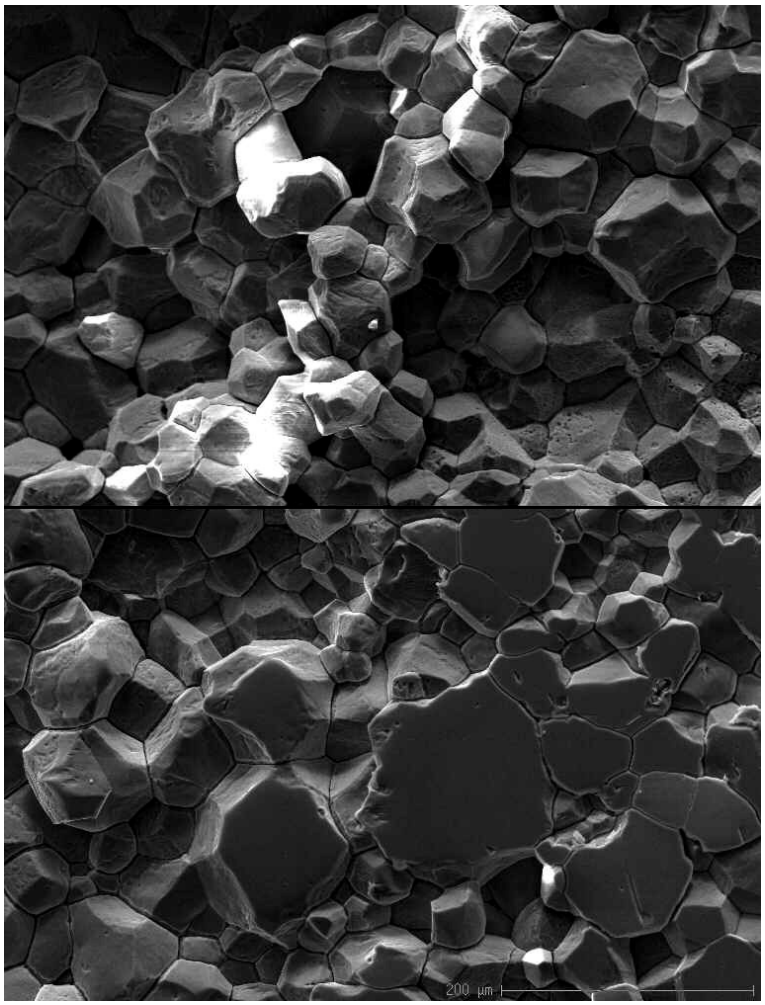

Figure 2.2: Scanning Electron Microscopy (SEM) images of an aluminium alloy that has been gallium etched to reveal its grain structure. Image from website of the National Physical Laboratory, Teddington, Middlesex, UK.

easier. Therefore interstitial diffusion is usually much faster than substitutional diffusion.

2.3.3 Diffusion in dilute solutions

We can imagine that interstitial (solute) atoms can travel trough the lattice without altering the solvent concentration levels; interstitial diffusion does not require the solvent atoms to change positions. For substitutional diffusion this is no longer the case; movement of solute atoms to one side usually involves movement of solvent atoms to the other. Fortunately, according to Porter and Easterling [1981] in sufficiently dilute solutions we may assume a constant solvent concentration level. According to Porter and Easterling [1981], this implies

we may use Fick's second law to model the diffusion process.

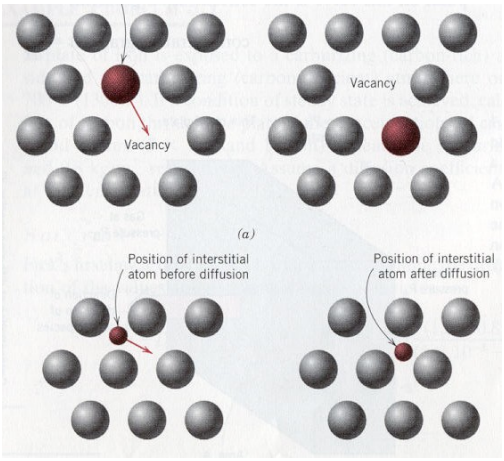

Figure 2.3: Interstitial and substitutional diffusion. Image source: Callister [1999].

2.4 Interphase interfaces

2.4.1 Gibbs-Thomson effect

We have seen that multiple phases of an alloy can co-exist in a piece of material. Often the crystal structures of these phases are not identical. The difference in crystal structure puts an extra strain on the inner phase. The most important consequence is that the Gibbs free energy inside the enclosed phase is raised. By utilizing the lever rule[1] we see that this results in a higher solubility at the matrix-precipitate interface. We call this phenomenon capillarity or the *Gibbs-Thomson effect*.

2.4.2 Interface migration

As a particle dissolves, its volume decreases; the interface will migrate inbound. Let us consider a B-rich particle inside an Al-rich grain. When the particle dissolves, B-atoms must cross the interface from the B-rich phase to the Al-rich phase. We call this the *interface reaction*. Once this atom has crossed the interface, the concentration of B in the Al-rich phase close to the interface has increased. In order to sustain the dissolution process the B-atoms need to move away from the interface to make room for new B-atoms. We call this the *long-distance diffusion* process. According to Vermolen [1998] the rate of dissolution in aluminium alloys is in practice governed by the long-distance

[1]Equilibrium between two phases requires that each component has the same chemical potential in each phase. The chemical potential can be obtained by extrapolating the tangent to the free energy curve to the sides of the molar energy diagram (hence, the 'lever rule'). See Chapter 1 of Porter and Easterling [1981] for more details.

diffusion process. This means that at the interface the components will be mixed according to thermodynamic equilibrium.

2.5 Nucleation

If a solid is heated or cooled to a temperature where the current phase is no longer stable, a driving force for a phase transformation exists. One type of phase transformation is the formation of precipitates. One might expect that the material would spontaneously transform to the new, more stable phase. This is, however, not the case; all precipitation phenomena start by the formation of very small particles, or *nuclei*, of the new phase. This process is called *nucleation*. Two different types of nucleation can be distinguished. We have *heterogeneous nucleation*, which occurs at defects (i.e. local imperfections in the material). *Homogeneous nucleation* occurs when no such imperfections are present. Because heterogeneous nucleation can destroy a defect –and release the increased free energy caused at such a defect– the net energy required for heterogeneous nucleation is lower than for homogeneous nucleation. Therefore almost all nucleation in solids occurs heterogeneously. More extensive information on nucleation theory can be found in Porter and Easterling [1981].

Chapter 3

Modeled homogenization phenomena

As we have discussed before, we know that the aluminium ingot or billet consists of microscopic grains. A schematic overview of such a grain is shown in Figure 3.1. The grain consists of several alloying elements. By far, the most

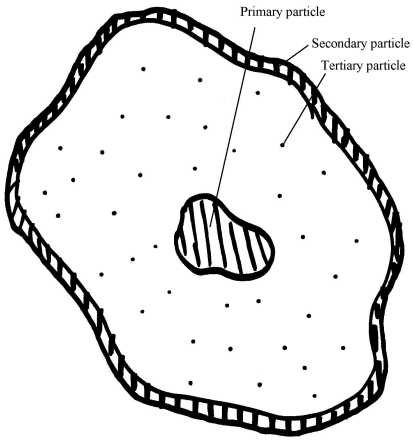

Figure 3.1: Schematic view of an aluminium grain.

common element will be aluminium since we are investigating aluminium alloys. In addition, several other alloying elements will be present in the grain. Some of these impurities are put in on purpose to improve the material characteristics of the alloy. Others are contaminants that are simply unavoidable. We will assume in our model that the concentration of aluminium is much larger than that of any of the other alloying elements.

The main problem -and the one under investigation- is that the alloying elements are not homogeneously distributed over the grain. The largest part of the grain is structured in the form of an aluminium-rich phase which is also referred to as the *solvent phase*. In this phase the concentration of aluminium is

–as the name suggests– relatively high, and the concentration of other elements is relatively low.

Now the grain also contains secondary phases that are low on aluminium and rich on other components. In the center of the grain we have a secondary phase in the shape of a (micrometer scale) precipitate that consists mainly of non-aluminium alloying elements. This particle will be referred to as a *primary particle*.

Additionally, we have another phase at the outer edge of the grain. This segregation layer consists of particles that have formed after casting during the cooling process. These particles need not have the same composition as the precipitate in the centre. We will refer to these precipitates as *secondary particles*.

During the heat treatment very small (nanometer scale) precipitates develop because of the nucleation process. We will call these *tertiary particles*.

3.1 Primary and secondary particle dissolution

The goal of the homogenization process is to (partly) dissolve the primary and/or secondary particles in order to improve the material properties of the alloy. Below it will be demonstrated how the theory from the previous chapter is applied in order to model this dissolution process. For the construction of our model, the following a-priori assumptions are made.

1. The concentration of alloying components is "low".
2. Diffusion only takes place inside the Al-rich phase. Precipitate phases are diffusion-free.
3. Precipitates are assumed to be of uniform, stoichiometric composition.

We will consider an aluminium alloy which contains N_p non-aluminium components. We need to model diffusion in the solvent phase only and we will designate this region with $\Omega(t)$. Note that since we have to deal with moving boundaries, the solvent phase geometry depends on time.

3.1.1 Component transfer inside the Al-rich phase

The alloying elements travel through the Al-rich phase under the influence of diffusion. Some alloying elements move more easily than others, so each is controlled by its own diffusion equation. Hence, for every $p \in P = \{1, \ldots, N_p\}$

$$\frac{\partial c_p(x,t)}{\partial t} = \nabla \cdot (D_p(T) \nabla c_p(x,t)) \qquad \text{for } x \in \Omega(t), t \in (0, \infty), \tag{3.1}$$

where

$$\begin{aligned} c_p &= \text{the solute concentration at position } x \text{ and time } t, \\ D_p &= \text{the diffusion coefficient of alloying element } p. \end{aligned}$$

According to Callister [1999] we may approximate the diffusion coefficient using the following formula

$$D_p(T) = D_{0,p} \exp\left(-\frac{Q_{d,p}}{RT}\right), \tag{3.2}$$

where

$$\begin{aligned} D_{0,p} &= \text{a temperature-independent pre-exponential,} \\ Q_{d,p} &= \text{the activation energy for diffusion,} \\ R &= \text{the gas constant,} \\ T &= \text{absolute temperature.} \end{aligned}$$

3.1.2 Initial condition

Before we can say anything about the kinetics of the particle dissolution, we must choose a starting situation. The Al-rich phase geometry at the start time is referred to as $\Omega(0)$. We use the following initial condition to define the concentration profile in the Al-rich phase at the beginning of our simulation:

$$c_p(x, 0) = c^0(x) \qquad \text{for } x \in \Omega(0). \tag{3.3}$$

3.1.3 Boundary conditions

We have now defined how matter is transported through the Al-rich phase, but we have yet to define what happens at the boundaries of our system. As said before, all the action takes place inside the grain, without any interaction with neighbouring grains. So if no segregation layer is present (anymore), a no-flux condition is governing component transfer at the grain boundary. Assuming precipitation nor dissolution is taking place at the boundary we conclude that this type of boundary does not move. On the other hand, if a segregation layer is present at the grain boundary or a precipitate is present in the centre of the grain, these secondary phases will most likely attempt to dissolve or grow. This results in a net movement of the interfaces separating the Al-rich phase from the secondary phases. Since we assume that diffusion only takes place within the solvent phase, these interfaces are effectively the boundaries of our problem, hence we need to define boundary conditions for them. Since they are moving, handling them will be somewhat more complex than for fixed boundaries. Moving boundaries are written as $S(t)$, fixed boundaries are written as Γ. $S(0)$ represents the position of the boundary at $t = 0$.

Fixed boundaries

We assume that during homogenization the grain size does not change. This means that no matter is exchanged with neighbouring grains at any time. Since this type of boundary does not move, we will call these fixed boundaries. This gives raise to the Neumann condition

$$\frac{\partial c_p(x, t)}{\partial n} = 0 \qquad \text{for } x \in \Gamma, t \in (0, \infty). \tag{3.4}$$

The n is defined as the normal unit vector pointing out of $\Omega(t)$.

Moving boundaries

A different type of boundary occurs at the interface that separates the phases in the grain. As a secondary phase releases the atoms inside it, the volume of this

phase decreases. We need to account for this process in our model. We assume that the dissolution process is diffusion-controlled, hence we assume that the material is always at its thermodynamic equilibrium at the solvent/precipitate phase interface. This means that our boundary condition is

$$c_p(x,t) = c_p^{\mathrm{sol}}(x,t) \qquad \text{for } x \in S(t), t \in (0,\infty). \tag{3.5}$$

Since we assume that the particle is, and remains stoichiometric (c_p^{part} constant for every $p \in P$), we can use the Gibbs free energy of the stoichiometric compound to obtain

$$\prod_{p\in P} \left(c_p^{\mathrm{sol}}(x,t)\right)^{m_p} = K(T) \qquad \text{for } x \in S(t), t \in (0,\infty). \tag{3.6}$$

Here m_p represents the multiplicity of the component in the stoichiometric compound. $K(T)$ is called the solubility product; it determines to what extent the different components can be dissolved in the solvent phase. Stoichiometry means that the composition of the secondary phase will remain the same. The balance of atoms leads to the following equation

$$v_n(x,t) = \frac{D_p}{c_p^{\mathrm{part}} - c_p^{\mathrm{sol}}(x,t)} \frac{\partial c_p}{\partial n}(x,t) \qquad \text{for } x \in S(t), t \in (0,\infty). \tag{3.7}$$

The moving boundary problem given by Equations (3.1)–(3.7) is known as a Stefan problem. More information about the mathematical properties of such a problem can be found in Section 4.

3.2 Tertiary particle precipitation

The creation of secondary particles proceeds in three stages: nucleation, growth and coarsening. In reality all three of these processes can take place inside the material at the same time. We will assume that the following holds:

1. All nucleation is of the heterogeneous type.
2. Precipitates are assumed to be of uniform composition. If temperature changes give raise to a change in composition, this change will happen instantaneously i.e. the precipitates are in thermodynamic equilibrium at all times.
3. All particles are assumed spherical.
4. A "steady-state diffusion field" is assumed around the particles, i.e. Fick's first law of thermodynamics applies.
5. Soft impingement does not occur. Diffusion fields of particles do not interact. This implies a dilute concentration of solute.

3.2.1 Nucleation

According to Russel [1970], to predict the number of nuclei that are produced heterogeneously in a system we may use

$$J = J_0 \exp\left(-\frac{\Delta G^*_{\mathrm{het}}}{RT}\right) \exp\left(-\frac{Q_d}{RT}\right), \tag{3.8}$$

where

$$J_0 = \text{a numerical constant},$$
$$\Delta G^*_{\text{het}} = \text{the energy barrier for nucleation}.$$

If the effect of elastic coherency strains can be ignored (i.e. the increase of Gibbs free energy in the particle due to misfit strain), then according to Myhr and Grong [2000]

$$\Delta G^*_{\text{het}} = \frac{(A_0)^3}{(RT)^2 \left(\ln(C_m/C_e)\right)^2}, \tag{3.9}$$

where

$$A_0 = \text{a value related to the energy barrier for nucleation},$$
$$C_m = \text{the mean solute concentration in the solvent phase},$$
$$C_e = \text{the equilibrium solute concentration at the interface}.$$

Combining the last two equations gives us

$$J = J_0 \exp\left[-\left(\frac{A_0}{RT}\right)^3 \left(\frac{1}{\ln(C_m/C_e)}\right)^2\right] \exp\left(-\frac{Q_d}{RT}\right). \tag{3.10}$$

3.2.2 Growth rate

As mentioned at the start of this paragraph, particle growth/dissolution is governed by a steady-state diffusion field. This means that the rate at which the radius of a spherical particle with radius r grows, is given by

$$v = \frac{dr}{dt} = \frac{C_m - C_i}{C_p - C_i}\frac{D}{r}, \tag{3.11}$$

in which C_i is the interface solute concentration and C_p is the particle solute concentration. Because the particles are very small we must take capillarity into account, hence

$$C_i = C_e \exp\left(\frac{2\sigma V_m}{rRT}\right), \tag{3.12}$$

in which σ is the interface energy and V_m is the molar volume of the particle. We can deduce the critical radius (i.e. the radius at which a particle neither grows nor shrinks) from the above equations by solving $v(r) = 0$. We now obtain

$$r^* = \frac{2\sigma V_m}{RT}\left(\ln\left(C_m/C_e\right)\right)^{-1}. \tag{3.13}$$

For $r < r^*$ we have $v < 0$, so a particle smaller than the critical radius will be unstable and dissolve. On the other hand, for $r > r^*$ we have $v > 0$ and thus a particle larger than the critical radius will grow.

3.2.3 Coarsening

The coarsening stage is handled naturally by the described nucleation model. As the solvent phase is depleted of solute and the concentration decreases, the critical radius will increase. This results in smaller particles dissolving and the larger ones growing. We do not need to make any special arrangements in our model to accommodate this behaviour.

3.2.4 Particle size distribution

Even in a volume as small as a grain, a very large number of nuclei can form. This means that it is not feasible to solve a diffusion equation for all the particles present in a single grain. Hence we will need to simplify our model a little. Our primary tool in reducing the workload is the *particle size distribution*. This approach is based on the numerical framework in Myhr and Grong [2000]. Instead of tracking each particle individually, we track classes of particles that are of the same size. The particle size distribution φ is defined as follows[1]

$$\#\text{ particles}/m^3 \text{ with } r_{\min} \leq \text{particle radius} \leq r_{\max} = \int_{r=r_{\min}}^{r_{\max}} \varphi(r,t)\,dr. \quad (3.14)$$

The flow of particles through the size classes can be modeled as a convection problem. Using the continuity equation we can show that the size distribution is controlled by the differential equation

$$\frac{\partial \varphi}{\partial t} = -\frac{\partial(\varphi v)}{\partial r} + S. \quad (3.15)$$

In this formula, v is the growth rate as defined above, and S is a source term due to the nucleation of new particles. We note that because of the dependence of v on C_m, and the dependence of C_m on φ (see below), the above equation is in fact nonlinear (in φ).

Since we are dealing with a convection problem that contains only outflow boundaries, we do not need to define any boundary conditions; only an initial condition is necessary.

3.2.5 Balance of mass

It is obvious that for every amount of material added to a particle when it grows, an equal amount of material is removed from the solvent phase. Application of a mass balance results in the equation

$$C_m = C_0 - (C_p - C_m) \int_{r=0}^{\infty} \frac{4}{3}\pi r^3 \varphi\,dr. \quad (3.16)$$

3.2.6 Particle volume fraction

The volume occupied by the nuclei in relation to the total volume is called the *particle volume fraction* and can be written as

$$f = \frac{C_0 - C_m}{C_p - C_m}. \quad (3.17)$$

[1] In Myhr and Grong [2000], the number of particles in a size class is tracked instead of the particle density.

Chapter 4

Stefan problems

The special class of moving boundary problems are commonly called Stefan problems. To gain some insight in the properties of this type of problems we will investigate the standard Stefan problem from a mathematical point of view. Vermolen [1998] contains some interesting results. We will demonstrate some important properties of the Stefan problem. For demonstration purposes we will use a simplified version of Equations (3.1–3.7).

The transport of the second phase in a finite matrix, $G(t) = (S(t), M)$ with $S(t)$ the moving boundary and M the fixed boundary, is described by:

$$\frac{\partial c(r,t)}{\partial t} = D\frac{\partial^2 c(r,t)}{\partial r^2} \qquad \forall r \in G(t), t \in (0, t_{\max}) \tag{4.1}$$

in which $c(r,t)$ is continuous, and has continuous derivatives with respect to t and r. Also $\frac{\partial c(r,t)}{\partial t}$ is continuous with a continuous derivative with respect to r. On the interface $S(t)$ we assume a constant Dirichlet condition, represented by:

$$c(S(t),t) = c^{\text{sol}} \qquad \forall t \in (0, t_{\max}). \tag{4.2}$$

At the other boundary, M, we have a homogeneous Neumann condition:

$$\frac{\partial c(M,t)}{\partial r} = 0 \qquad \forall t \in (0, t_{\max}). \tag{4.3}$$

The initial concentration is known and is given by the constant c^0:

$$c(r,0) = c^0 \qquad \forall r \in G(0). \tag{4.4}$$

The interface between the second phase and the primary phase, $S(t)$, moves due to the balance of mass, and this yields:

$$\int_{r=0}^{M} c(r,t)\,dr = c^{\text{part}} \cdot S(t) + \int_{r=S(t)}^{M} c(r,t)\,dr = \overline{c} \cdot M, \tag{4.5}$$

where $\overline{c}$ represents the average concentration. If Equation (4.3) holds, $\overline{c}$ is constant and it can be proved by differentiation of Equation (4.5) and using Equation (4.1), that Equation (4.5) is equivalent to

$$\frac{dS(t)}{dt} = \frac{D}{c^{\text{part}} - c^{\text{sol}}}\frac{\partial c(S(t),t)}{\partial t}. \tag{4.6}$$

Either of Equations (4.5) and (4.6) may be used to determine the position of the free boundary.

4.1 Maximum principle

The maximum principle is a well-known result in the study of parabolic differential equations. A proof of this property is given in Protter and Weinberger [1967]. Without proof, we will give the following result.

Proposition 4.1.1. *The global extremes of a solution to the diffusion equation must occur either at the boundaries S_1, S_2 or at $t = 0$.*

4.2 Equivalence of integral and differential form of Stefan condition

Proposition 4.2.1. *Only if the Neumann boundary condition at M is homogeneous, then Equations* (4.5) *and* (4.6) *are equivalent.*

$$\int_{r=0}^{M} c(r,t)\,dr = c^{\text{part}} S(t) + \int_{r=S(t)}^{M} c(r,t)\,dr = \bar{c}\cdot M \Leftrightarrow \frac{dS(t)}{dt} = \frac{D}{c^{\text{part}} - c^{\text{sol}}} \frac{\partial c(S(t),t)}{\partial r}$$

with $\bar{c}$ the average concentration. The intermediate value theorem for integrals postulates that $\bar{c} \in \left(\min_{r\in(0,M)} c(r,t), \max_{r\in(0,M)} c(r,t)\right)$.

Proof. The first part of the proposition will be proved first. Differentiation of Equation (4.5) with respect to time, while using that $\bar{c} =$ constant, yields

$$\begin{aligned} &c^{\text{part}} \frac{dS(t)}{dt} + \frac{d}{dt}\int_{r=S(t)}^{M} c(r,t)\,dr = \\ &\quad c^{\text{part}} \frac{dS(t)}{dt} + \frac{dS(t)}{dt}\frac{d}{dS(t)}\int_{r=S(t)}^{M} c(r,t)\,dr + \int_{r=S(t)}^{M} \frac{\partial c(r,t)}{\partial t}\,dr = 0. \end{aligned} \quad (4.7)$$

As the derivative of an integral with respect to the boundary equals the value of the integrand at the boundary, we obtain

$$(c^{\text{part}} - c^{\text{sol}})\frac{dS(t)}{dt} = -\int_{r=S(t)}^{M} \frac{\partial c(r,t)}{\partial t}\,dr = -D\int_{r=S(t)}^{M} \frac{\partial^2 c(r,t)}{\partial r^2}\,dr = D\frac{\partial c(S(t),t)}{\partial r}. \quad (4.8)$$

In the last step, the homogeneous Neumann condition has been used. If the Neumann condition were not homogeneous, then a term with the concentration gradient at M has to be added. For the case of a homogeneous Neumann condition at M it has been proved that Equation (4.5) implies Equation (3.7). The steps in the proof are equivalences, if and only if there is a homogeneous Neumann condition at M. □

4.3 Ill-posed Stefan problems

The Stefan problem can not always be solved reliably. The first problem we observe is when the interface concentration is equal to the particle concentration, i.e. $c_p^{\text{part}} = c_{p,k}^{\text{sol}}(t)$. Then we can no longer derive the interface movement from Equation (3.7). The second issue occurs when the initial matrix concentration is equal to the particle concentration. Both observations can be proved by use of the following proposition:

Proposition 4.3.1. *The problem as constituted by Equations* (4.1)–(4.5) *has no real solution if* $\left(c^{\text{part}} - c^0\right)\left(c^{\text{part}} - c^{\text{sol}}\right) < 0$.

Proof. Equations (4.1)–(4.5) imply a homogeneous Neumann boundary condition at M. Suppose that a solution exists for equations. From Proposition 4.2.1 follows that Equations (4.5) and (4.6) are equivalent. Equation (4.5) may be written as: $\int_{r=0}^{M} c(r,t)\,dr = \overline{c} \cdot M$. As $\left(c^{\text{part}} - c^0\right)\left(c^{\text{part}} - c^{\text{sol}}\right) < 0 \Leftrightarrow (c^0 < c^{\text{part}} < c^{\text{sol}}) \vee (c^{\text{sol}} < c^{\text{part}} < c^0)$, we first consider the case that $(c^0 < c^{\text{part}} < c^{\text{sol}})$. From the maximum principle of the diffusion equation follows that for this case $\frac{\partial c(S(t),t)}{\partial r} < 0$. Since $c^{\text{part}} < c^{\text{sol}}$, it follows that $\frac{dS(t)}{dt} > 0$. Considering $t = 0$, we have for the global mass: $S_0 \cdot c^{\text{part}} + (M - S_0) \cdot c^0 = \overline{c} \cdot M$. For $t = dt$, we have for the global mass:

$$\begin{aligned}
&S(dt) \cdot c^{\text{part}} + \int_{r=S(dt)}^{M} c(r,t)\,dr \\
&= S(0) \cdot c^{\text{part}} + (S(dr) - S(0)) \cdot c^{\text{part}} + \int_{r=S(dt)}^{M} c(r,t)\,dr \\
&= S(0) \cdot c^{\text{part}} + \int_{r=S(0)}^{M} c(r,t)\,dr
\end{aligned}$$

From the maximum principle of the diffusion equation follows $c(r,t) \geq c^0$ and from $c(r,t) = c^{\text{part}} > c^0$ for $r \in (S_0, S(dt))$ it is clear that

$$S(0) \cdot c^{\text{part}} + \int_{r=S(0)}^{M} c(r,t)\,dr > S(0) \cdot c^{\text{part}} + \int_{r=S(0)}^{M} c(r,0)\,dr = \overline{c} \cdot M,$$

implying that Equations (4.5) and (4.6) are not equivalent. The problem with $(c^0 < c^{\text{part}} < c^{\text{sol}})$ and a homogeneous Neumann condition at M does not have a real solution. A similar proof can be given to show that for the case $(c^{\text{sol}} < c^{\text{part}} < c^0)$ no real solution exists. Then we can show that $S(dt) \cdot c^{\text{part}} + \int_{r=S(dt)}^{M} c(r,t)\,dr < M \cdot \overline{c}$. □

Chapter 5

Numerical solution methods

Now that we have constructed a model of the homogenization process, we would like to see how we can apply it to a test problem. We have to approximate the solution by using a numerical method. As usual, no one-size-fits-all solution exists and we need to decide in what way we will calculate our desired solution.

5.1 Geometry

Before we can start solving the problem, we need to define the geometry. We will perform all calculations on a cylindrical or spherical geometry. A schematic overview of the cylindrical geometry is shown in Figure 5.1. Switching between cylindrical and spherical geometries is trivial by the use of a geometric parameter a. In the center we can see the primary precipitate and at the edge we see the segregation layer. We can use the symmetry of this geometry to reduce the Stefan problem to a one-dimensional moving boundary problem.

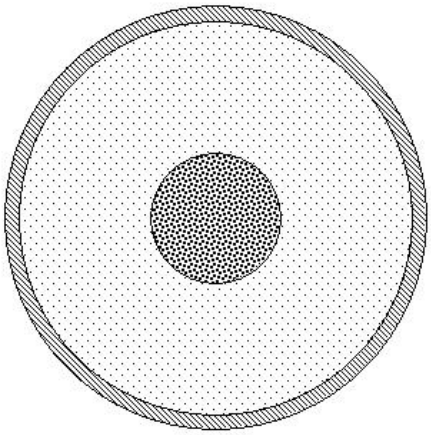

Figure 5.1: Schematic view of a grain in cylindrical geometry. Primary and secondary particles are present as well.

5.2 Primary and secondary particle dissolution

To solve the one-dimensional Stefan problem we will use the moving mesh method described in Vermolen [1998]. The outline for our algorithm is as follows:

1. Compute the concentration profiles solving the nonlinear problem given by Equations (3.1)–(3.7),
2. Predict the positions of S_1 and S_2 at the new time-step: $S_1(t+\Delta t)$ and $S_2(t+\Delta t)$, using Equation (3.7),
3. Redistribute the grid such that $S_1(t+\Delta t)$ and $S_2(t+\Delta t)$ are nodal points,
4. Return to step 1.

5.2.1 Discretisation of the interior region

We need to solve a diffusion equation for every component in our system, but for brevity the dependence on p is not shown in the equations below, so where you see c_i^j, please read $c_{p,i}^j$. To reduce our continuous problem to a system of linear equations, we use the finite volume method as follows. We start by taking Equation (3.1):

$$r^a \frac{\partial c}{\partial t} = \frac{\partial}{\partial r}\left\{ D r^a \frac{\partial c}{\partial r} \right\}.$$

Integrating on both sides with respect to space and time gives

$$\int_{t^j}^{t^{j+1}} \int_{r_{i-\frac{1}{2}}^{j+1}}^{r_{i+\frac{1}{2}}^{j+1}} r^a \frac{\partial c}{\partial t} dr dt = \int_{t^j}^{t^{j+1}} \int_{r_{i-\frac{1}{2}}^{j+1}}^{r_{i+\frac{1}{2}}^{j+1}} \frac{\partial}{\partial r}\left\{ D r^a \frac{\partial c}{\partial r} \right\} dr dt.$$

Left hand side

$$\begin{aligned}
\int_{t^j}^{t^{j+1}} \int_{r_{i-\frac{1}{2}}^{j+1}}^{r_{i+\frac{1}{2}}^{j+1}} r^a \frac{\partial c}{\partial t} dr dt &= \int_{t^j}^{t^{j+1}} \frac{\partial}{\partial t} \int_{r_{i-\frac{1}{2}}^{j+1}}^{r_{i+\frac{1}{2}}^{j+1}} r^a c \, dr dt \\
&\approx \int_{t^j}^{t^{j+1}} \frac{\partial}{\partial t} \left[\left(r_i^{j+1} \right)^a \left(r_{i+\frac{1}{2}}^{j+1} - r_{i-\frac{1}{2}}^{j+1} \right) c\left(r_i^{j+1}, t \right) \right] dt \\
&\approx \left(r_i^{j+1} \right)^a \left(r_{i+\frac{1}{2}}^{j+1} - r_{i-\frac{1}{2}}^{j+1} \right) \left[c\left(r_i^{j+1}, t^{j+1} \right) - c\left(r_i^{j+1}, t^j \right) \right]
\end{aligned}$$

Using Taylor's theorem we approximate

$$\begin{aligned}
c\left(r_i^{j+1}, t^j \right) &\approx c\left(r_i^j, t^j \right) + \left(r_i^{j+1} - r_i^j \right) \frac{\partial c}{\partial r}\left(r_i^j, t^j \right) \\
&\approx \left(r_i^j, t^j \right) + \left(r_i^{j+1} - r_i^j \right) \frac{c\left(r_{i+1}^j, t^j \right) - c\left(r_{i-1}^j, t^j \right)}{r_{i+1}^j - r_{i-1}^j}.
\end{aligned}$$

Right hand side

$$\begin{aligned}
&\int_{t^j}^{t^{j+1}} \int_{r_{i-\frac{1}{2}}^{j+1}}^{r_{i+\frac{1}{2}}^{j+1}} \frac{\partial}{\partial r}\left\{ Dr^a \frac{\partial c}{\partial r} \right\} dr dt \\
&= \int_{t^j}^{t^{j+1}} Dr^a \frac{\partial c}{\partial r}\Big|_{(r_{i-\frac{1}{2}}^{j+1},t)}^{(r_{i+\frac{1}{2}}^{j+1},t)} dt \\
&= \int_{t^j}^{t^{j+1}} \left[\left(Dr^a \frac{\partial c}{\partial r} \right)\left(r_{i+\frac{1}{2}}^{j+1}, t \right) - \left(Dr^a \frac{\partial c}{\partial r} \right)\left(r_{i-\frac{1}{2}}^{j+1}, t \right) \right] dt \\
&\approx \left[\left(Dr^a \frac{\partial c}{\partial r} \right)\left(r_{i+\frac{1}{2}}^{j+1}, t^{j+1} \right) - \left(Dr^a \frac{\partial c}{\partial r} \right)\left(r_{i-\frac{1}{2}}^{j+1}, t^{j+1} \right) \right] \left(t^{j+1} - t^j \right),
\end{aligned}$$

in which

$$\begin{aligned}
\left(Dr^a \frac{\partial c}{\partial r} \right)\left(r_{i+\frac{1}{2}}^{j+1}, t^{j+1} \right) &= D(r_{i+\frac{1}{2}}^{j+1}, t^{j+1}) \left(r_{i+\frac{1}{2}}^{j+1} \right)^a \frac{\partial c}{\partial r}(r_{i+\frac{1}{2}}^{j+1}, t^{j+1}) \\
&\approx D(r_{i+\frac{1}{2}}^{j+1}, t^{j+1}) \left(r_{i+\frac{1}{2}}^{j+1} \right)^a \frac{c(r_{i+1}^{j+1}, t^{j+1}) - c(r_i^{j+1}, t^{j+1})}{r_{i+1}^{j+1} - r_i^{j+1}}
\end{aligned}$$

and

$$\begin{aligned}
\left(Dr^a \frac{\partial c}{\partial r} \right)\left(r_{i-\frac{1}{2}}^{j+1}, t^{j+1} \right) &= D(r_{i-\frac{1}{2}}^{j+1}, t^{j+1}) \left(r_{i-\frac{1}{2}}^{j+1} \right)^a \frac{\partial c}{\partial r}(r_{i-\frac{1}{2}}^{j+1}, t^{j+1}) \\
&\approx D(r_{i-\frac{1}{2}}^{j+1}, t^{j+1}) \left(r_{i-\frac{1}{2}}^{j+1} \right)^a \frac{c(r_i^{j+1}, t^{j+1}) - c(r_{i-1}^{j+1}, t^{j+1})}{r_i^{j+1} - r_{i-1}^{j+1}}.
\end{aligned}$$

For our convenience we will introduce the shorthand notations

$$\begin{aligned}
c_i^j &= c(r_i^j, t^j), \\
D_i^j &= D(r_i^j, t^j).
\end{aligned}$$

We now get the following set of equations:

$$\begin{aligned}
&\left(r_i^{j+1} \right)^a \left(r_{i+\frac{1}{2}}^{j+1} - r_{i-\frac{1}{2}}^{j+1} \right) \left(c_i^{j+1} - c_i^j - (r_i^{j+1} - r_i^j) \frac{c_{i+1}^j - c_{i-1}^j}{r_{i+1}^j - r_{i-1}^j} \right) \\
&= \left(D_{i+\frac{1}{2}}^{j+1} \left(r_{i+\frac{1}{2}}^{j+1} \right)^a \frac{c_{i+1}^{j+1} - c_i^{j+1}}{r_{i+1}^{j+1} - r_i^{j+1}} - D_{i-\frac{1}{2}}^{j+1} \left(r_{i-\frac{1}{2}}^{j+1} \right)^a \frac{c_i^{j+1} - c_{i-1}^{j+1}}{r_i^{j+1} - r_{i-1}^{j+1}} \right) (t^{j+1} - t^j).
\end{aligned}$$

By reordering the terms we get an expression of the form

$$\alpha_{i-1}^{j+1} c_{i-1}^{j+1} + \alpha_i^{j+1} c_i^{j+1} + \alpha_{i+1}^{j+1} c_{i+1}^{j+1} = \beta_i^{j+1},$$

in which

$$\alpha_{i,i-1}^{j+1} = -\frac{D_{i-\frac{1}{2}}^{j+1}\left(r_{i-\frac{1}{2}}^{j+1}\right)^a}{r_i^{j+1} - r_{i-1}^{j+1}} \tag{5.1}$$

$$\alpha_{i,i}^{j+1} = \frac{D_{i+\frac{1}{2}}^{j+1}\left(r_{i+\frac{1}{2}}^{j+1}\right)^a}{r_{i+1}^{j+1} - r_i^{j+1}} + \frac{D_{i-\frac{1}{2}}^{j+1}\left(r_{i-\frac{1}{2}}^{j+1}\right)^a}{r_i^{j+1} - r_{i-1}^{j+1}} + \frac{\left(r_i^{j+1}\right)^a\left(r_{i+\frac{1}{2}}^{j+1} - r_{i-\frac{1}{2}}^{j+1}\right)}{t^{j+1} - t^j} \tag{5.2}$$

$$\alpha_{i,i+1}^{j+1} = -\frac{D_{i+\frac{1}{2}}^{j+1}\left(r_{i+\frac{1}{2}}^{j+1}\right)^a}{r_{i+1}^{j+1} - r_i^{j+1}} \tag{5.3}$$

$$\beta_i^{j+1} = \frac{\left(r_i^{j+1}\right)^a\left(r_{i+\frac{1}{2}}^{j+1} - r_{i-\frac{1}{2}}^{j+1}\right)}{t^{j+1} - t^j}\left(c_i^j + \frac{r_i^{j+1} - r_i^j}{r_{i+1}^j - r_{i-1}^j}\left(c_{i+1}^j - c_{i-1}^j\right)\right). \tag{5.4}$$

This equation holds for all $1 \leq i \leq n-1$.

5.2.2 Boundary conditions

We have found a set of equations that describe the diffusion of material inside the matrix. Now we need to define what happens on the boundaries.

Moving boundaries

Boundary conditions of the type of Equation (3.5) are easy to implement. All we need to do is eliminate the unknown by substituting the prescribed value in the discretisation derived in Equations (5.1)–(5.4), i.e. we substitute

$$c_0^{j+1} = c_{p,1}^{\text{sol}},$$

and/or

$$c_n^{j+1} = c_{p,2}^{\text{sol}},$$

depending on which side the moving boundary is at.

Fixed boundaries

Implementing the fixed boundaries, which have a condition as prescribed in Equation (3.4), is a little less straight-forward. Multiple approaches are possible. In the present case we will implement this type of boundary condition by adding a virtual point just beyond each boundary. Using the discrete version (according to finite differences) of Equation (3.4), we get

$$\frac{c_1^{j+1} - c_{-1}^{j+1}}{r_1^{j+1} - r_{-1}^{j+1}} = 0$$

and/or

$$\frac{c_{n+1}^{j+1} - c_{n-1}^{j+1}}{r_{n+1}^{j+1} - r_{n-1}^{j+1}} = 0,$$

again depending on which side the fixed boundary is at. We substitute this into Equations (5.1)–(5.4) to obtain the discrete equations for $i = 0$ or $i = n$.

5.2.3 Solving the nonlinear problem

What we have done above looks simple enough, but what we did not mention was that in the case of a moving boundary we do not know the value of $c_{p,k}^{\mathrm{sol}} = c_{p,k}^{j+1}$ as of yet. We need Equations (3.6) and (3.7) to determine this value. Because this is a nonlinear problem we proceed as follows. We assume two moving boundaries are present

1. Take a "good" first guess for $c_{p,0}^{j+1}$ and $c_{p,n}^{j+1}$.
2. Using the current estimates for $c_{p,0}^{j+1}$, $c_{p,n}^{j+1}$ and S_k^{j+1}, and the c_i^j and S_k^j from the previous time step, we can calculate the new concentration profiles for each component, as well as the concentration gradients at the boundaries.
3. Now we have enough information to do a Newton-Raphson step and obtain a (hopefully) better approximation for $c_{p,0}^{j+1}$ and $c_{p,n}^{j+1}$.
4. Continue with step 1 until the desired accuracy is reached.

5.2.4 Moving the boundary

As soon as we have found a set of component solubilities that satisfy all equations, we may proceed with moving the boundaries. Here, we take an explicit approach and use a discretized version of Equation (3.7) to determine the new position S_k^{j+2}.

5.3 Tertiary particle precipitation

For solving the nucleation problem we will use a finite volume method for the transport equation. First order upwind differencing will be used to approximate the fluxes at the cell boundaries. The algorithm can be outlined as follows (see also Myhr and Grong [2000]):

1. Calculate the nucleation rate, mean matrix concentration and velocity field from $\varphi(t - \Delta t)$, using Equations (3.10), (3.16) and (3.11).
2. Perform one implicit Euler time step for Equation (3.15) to find $\varphi(t)$.
3. Calculate and store statistics (e.g. volume fraction, mean radius etc.).
4. Repeat from step 1 until at end time.

5.3.1 Discretisation of the interior region

In order to solve the nucleation problem we need a discretized version of Equation (3.15). As mentioned before, due to the interdependence of φ, v and C_m, this is a nonlinear problem. Therefore we will only solve φ implicitly; C_m and v will be determined from the previous time step. We start by taking Equation (3.15):

$$\frac{\partial \varphi}{\partial t} = -\frac{\partial(\varphi v)}{\partial r} + S$$

Integrating both sides with respect to space and time gives

$$\int_{t^j}^{t^{j+1}} \int_{r_{i-\frac{1}{2}}}^{r_{i+\frac{1}{2}}} \frac{\partial \varphi}{\partial t}\, dr\, dt = -\int_{t^j}^{t^{j+1}} \int_{r_{i-\frac{1}{2}}}^{r_{i+\frac{1}{2}}} \frac{\partial}{\partial r}(\varphi v)\, dr\, dt + \int_{t^j}^{t^{j+1}} \int_{r_{i-\frac{1}{2}}}^{r_{i+\frac{1}{2}}} S\, dr\, dt.$$

Left hand side

$$\begin{aligned}\int_{t^j}^{t^{j+1}} \int_{r_{i-\frac{1}{2}}}^{r_{i+\frac{1}{2}}} \frac{\partial \varphi}{\partial t}\, dr\, dt &= \int_{t^j}^{t^{j+1}} \frac{\partial}{\partial t} \int_{r_{i-\frac{1}{2}}}^{r_{i+\frac{1}{2}}} \varphi\, dr\, dt \\ &\approx \int_{t^j}^{t^{j+1}} \frac{\partial}{\partial t} \left\{ \varphi(r_i, t)(r_{i+\frac{1}{2}} - r_{i-\frac{1}{2}}) \right\} dt \\ &\approx (\varphi(r_i, t^{j+1}) - \varphi(r_i, t^j))(r_{i+\frac{1}{2}} - r_{i-\frac{1}{2}})\end{aligned} \tag{5.5}$$

Right hand side

The right hand side of the equation consists of two terms. We will handle them one by one. The convection term becomes

$$\begin{aligned}\int_{t^j}^{t^{j+1}} \int_{r_{i-\frac{1}{2}}}^{r_{i+\frac{1}{2}}} \frac{\partial}{\partial r}(\varphi v)\, dr\, dt &= \int_{t^j}^{t^{j+1}} \left\{ (\varphi v)(r_{i+\frac{1}{2}}, t) - (\varphi v)(r_{i-\frac{1}{2}}, t) \right\} dt \\ &\approx \left((\varphi v)(r_{i+\frac{1}{2}}, t^{j+1}) - (\varphi v)(r_{i-\frac{1}{2}}, t^{j+1}) \right) (t^{j+1} - t^j).\end{aligned} \tag{5.6}$$

And for the source term we get

$$\begin{aligned}\int_{t^j}^{t^{j+1}} \int_{r_{i-\frac{1}{2}}}^{r_{i+\frac{1}{2}}} S\, dr\, dt &\approx \int_{t^j}^{t^{j+1}} S(r_i, t)(r_{i+\frac{1}{2}} - r_{i-\frac{1}{2}})\, dt \\ &\approx S(r_i, t^j)(r_{i+\frac{1}{2}} - r_{i-\frac{1}{2}})(t^{j+1} - t^j).\end{aligned} \tag{5.7}$$

Now we introduce the following shorthand notations:

$$\begin{aligned}\varphi_i^j &= \varphi(r_i, t^j) \\ v_i^j &= v(r_i, t^j) \\ v_{i+\frac{1}{2}}^j &= v(\frac{r_i + r_{i+1}}{2}, t^j) \\ (\varphi v)_i^j &= \varphi(r_i, t^j) \cdot v(r_i, t^j) \\ \Delta r_i &= r_{i+\frac{1}{2}} - r_{i-\frac{1}{2}} \\ \Delta t^{j+1} &= t^{j+1} - t^j\end{aligned}$$

Using a first order upwind discretisation, we get

$$\begin{aligned}(\varphi v)_{i+\frac{1}{2}}^{j+1} &= \begin{cases} v_{i+\frac{1}{2}}^j \varphi_i^{j+1}, & \text{if } v_{i+\frac{1}{2}}^j \geq 0 \\ v_{i+\frac{1}{2}}^j \varphi_{i+1}^{j+1}, & \text{otherwise} \end{cases} \\ &= \frac{1}{2}\left(v_{i+\frac{1}{2}}^j + |v_{i+\frac{1}{2}}^j| \right) \varphi_i^{j+1} + \frac{1}{2}\left(v_{i+\frac{1}{2}}^j - |v_{i+\frac{1}{2}}^j| \right) \varphi_{i+1}^{j+1}\end{aligned} \tag{5.8}$$

Combining Equations (5.5), (5.6), (5.7) and (5.8) results in the following system of equations.

$$\begin{aligned}\left(\varphi_i^{j+1} - \varphi_i^j\right)\Delta r_i = &-\frac{1}{2}\Delta t^{j+1}\left[\left(v^j_{i+\frac{1}{2}} + |v^j_{i+\frac{1}{2}}|\right)\varphi_i^{j+1} + \left(v^j_{i+\frac{1}{2}} - |v^j_{i+\frac{1}{2}}|\right)\varphi_{i+1}^{j+1}\right] \\ &+ \frac{1}{2}\Delta t^{j+1}\left[\left(v^j_{i-\frac{1}{2}} + |v^j_{i-\frac{1}{2}}|\right)\varphi_{i-1}^{j+1} + \left(v^j_{i-\frac{1}{2}} - |v^j_{i-\frac{1}{2}}|\right)\varphi_i^{j+1}\right] \\ &+ S_i^j \Delta r_i \Delta t^{j+1},\end{aligned}$$

which we can rewrite to

$$\alpha_{i-1}^{j+1}\varphi_{i-1}^{j+1} + \alpha_i^{j+1}\varphi_i^{j+1} + \alpha_{i+1}^{j+1}\varphi_{i+1}^{j+1} = \beta_i^{j+1},$$

in which

$$\begin{aligned}\alpha_{i-1}^{j+1} &= -\frac{\Delta t}{2\Delta r_i}\left(v^j_{i-\frac{1}{2}} + |v^j_{i-\frac{1}{2}}|\right) \\ \alpha_i^{j+1} &= 1 + \frac{\Delta t}{2\Delta r_i}\left[\left(v^j_{i+\frac{1}{2}} + |v^j_{i+\frac{1}{2}}|\right) - \left(v^j_{i-\frac{1}{2}} - |v^j_{i-\frac{1}{2}}|\right)\right] \\ \alpha_{i+1}^{j+1} &= \frac{\Delta t}{2\Delta r_i}\left(v^j_{i+\frac{1}{2}} - |v^j_{i+\frac{1}{2}}|\right) \\ \beta_i^{j+1} &= \varphi_i^j + \Delta t S_i^j\end{aligned}$$

As mentioned before, the values for $v^j_{i-\frac{1}{2}}$, $v^j_{i+\frac{1}{2}}$ and S_i^j are calculated from the previous time step. When combining Equations (3.11) and (3.12), we get

$$v_i^j = \frac{C_m^j - C_e^j \exp\left(\frac{2\sigma V_m}{r_i^j RT}\right)}{C_p - C_e^j \exp\left(\frac{2\sigma V_m}{r_i^j RT}\right)}\frac{D}{r_i^j}$$

From the mass balance (3.16), we get

$$C_m^j = \frac{C_0 - C_p f^j}{1 - f^j}$$

The volume fraction f^j can be approximated by

$$\begin{aligned}f^j &= \int_{r=0}^{\infty} \frac{4}{3}\pi r^3 \varphi^j \, dr \\ &\approx \sum_i \frac{4}{3}\pi (r_i)^3 \varphi_i^j.\end{aligned} \tag{5.9}$$

The source term S is related to the nucleation rate J in the following way

$$S_i^j = \begin{cases} \frac{J^j}{\Delta r_i}, & \text{if } r_{i-\frac{1}{2}} < 1.05 \times r^* \leq r_{i+\frac{1}{2}} \\ 0, & \text{otherwise.}\end{cases} \tag{5.10}$$

The factor 1.05 is to give the new particles a chance to grow.

5.3.2 Boundary conditions

Since we have a transport equation which has only outflow boundaries ($v(0,t) < 0$ and for $0 \leq r^* < r$ we have $v(r,0) > 0$), we do not need to define boundary conditions for them. We only need to give an initial condition for φ at $t = 0$. This initial size distribution is given by the function $\varphi^0(r)$, so we demand that

$$\varphi(r,0) = \varphi^0(r).$$

Chapter 6

Test cases

6.1 Primary and secondary particle dissolution

We checked the working of the solver for the Stefan problem by comparing the results of our solver to the results as presented in Vermolen [1998]. We will be running the program in a spherical geometry, with the parameters shown in Table 6.1. The concentration profile inside the grain is shown for various

Parameter	Unit	Value
D_C	m^2/s	$2 \cdot 10^{-13}$
D_B	m^2/s	$1 \cdot 10^{-13}$
c_p^0	%	0
c_p^{part}	%	50
K	-	1
M_1	m	0
$S_1(0)$	m	$7.5 \cdot 10^{-7}$
M_2	m	$5 \cdot 10^{-6}$
$M_2 - S_2(0)$	m	$2 \cdot 10^{-8}$
# volumes	-	500
Δt	s	5

Table 6.1: Input parameters

times in Figures 6.1 to 6.4. At $t = 5$, we see that the concentration levels in the solvent phase are rising. Strong concentration gradients make the particle and segregation layers dissolve fast. At $t = 10$ the concentration in the solvent phase has increased even more. As such, the concentration gradients at the moving boundaries become less pronounced; the dissolution process is slowing down. The segregation layer has almost dissolved. At $t = 100$ the segregation layer is gone, and the primary particle continues to dissolve at a constant rate. At $t = 250$, the concentration gradient at the remaining moving boundary starts to increase due to the decreasing area of the particle. The dissolution process speeds up again until the primary particle is dissolved. At $t = 300$ (not shown) the concentration is constant throughout the grain. The material is now homogeneous.

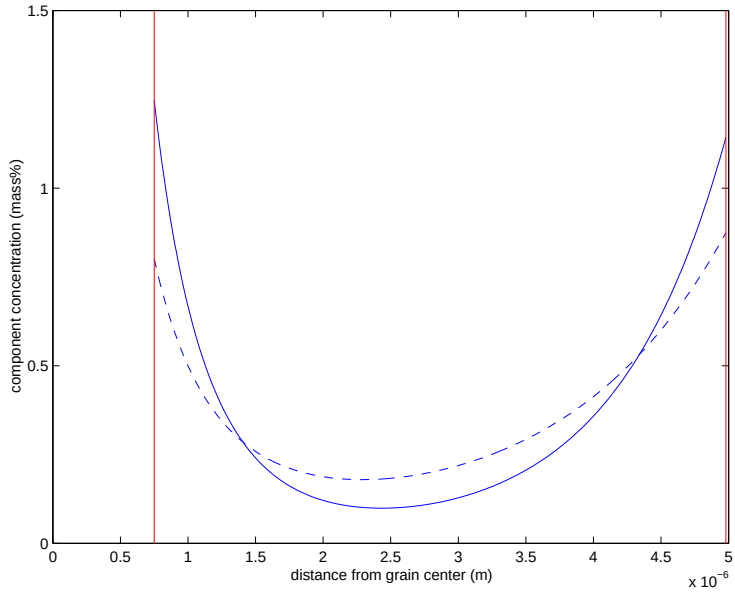

Figure 6.1: Particle dissolution at $t = 5$ s. The concentrations of elements B and C are represented by the solid and dashed lines, respectively.

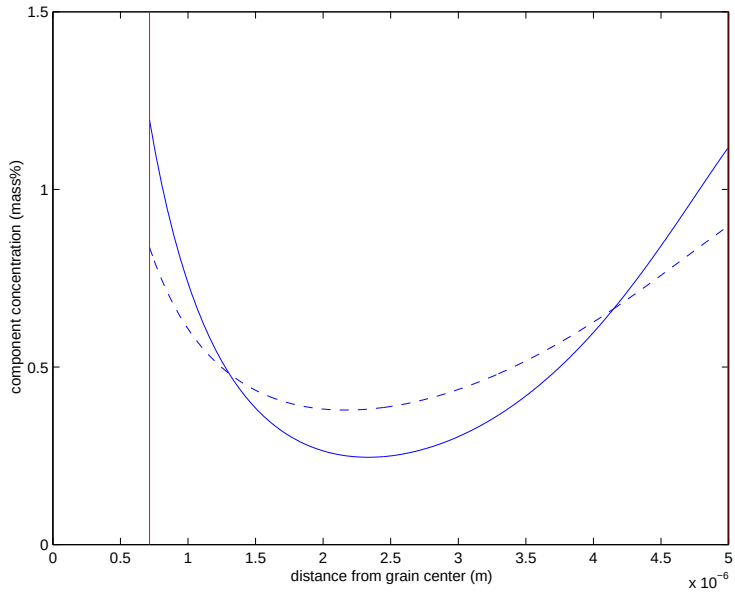

Figure 6.2: Particle dissolution at $t = 10$ s.

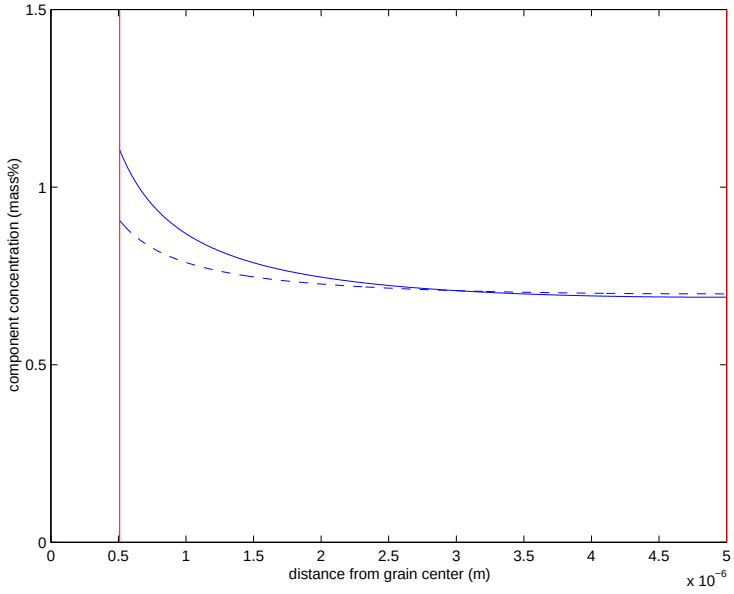

Figure 6.3: Particle dissolution at $t = 100$ s.

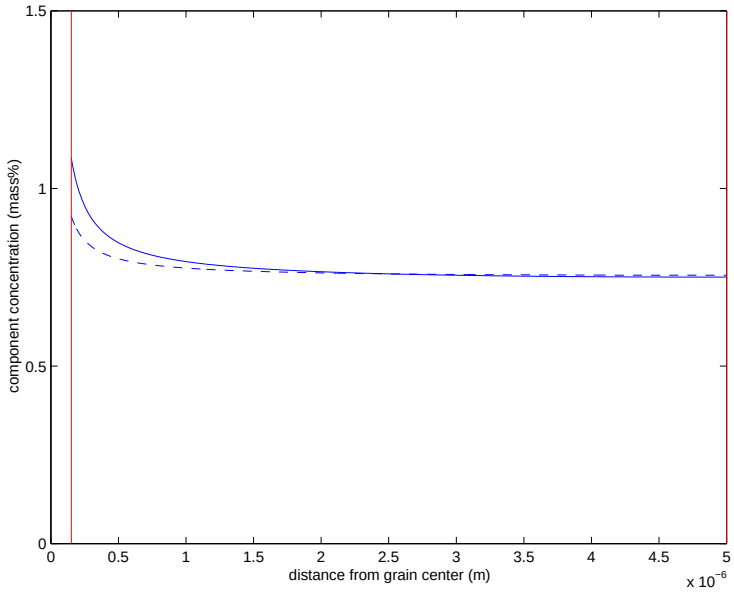

Figure 6.4: Particle dissolution at $t = 250$ s.

6.2 Tertiary particle precipitation

We test our derived nucleation model by comparing the results of our model to the results as shown in Myhr and Grong [2000]. The used input values can be found in Table 6.2. We will not attempt to reproduce all the results in

Parameter	Unit	Value
C_p	wt%	64.3
C_0	wt%	0.63
C_s	wt%	970
D_0	m^2/s	2.2×10^{-4}
A_0	J/mol	16220
j_0	$\#/m^3 s$	9.66×10^{34}
Q_d	J/mol	130000
Q_s	J/mol	47175
σ	J/m^2	0.2
V_m	m^3/mol	3.95×10^{-5}

Table 6.2: Input parameters

the aforementioned article. Instead we will only compare the results for the isothermal heat treatment. In this situation, a piece of AA 6082 aluminium alloy is held at a constant temperature of 180°C for 10^7 seconds ($\approx$ 115 days). We assume no precipitation is present at the beginning of the heat treatment thus the system is initially supersaturated. In Figures 6.5 to 6.9 the kinetics of the system during the heat treatment are displayed. This example was chosen because it is easy to identify the nucleation, growth and coarsening stages during the heat treatment.

During the first 10^3 seconds of the treatment, we see that the number of particles in the material climbs steadily (Figure 6.6). The particle volume fraction (Figure 6.5) and matrix concentration (Figure 6.8) do not change however. This indicates that during this time a lot of nuclei are added to the system, but they do not significantly alter the alloy composition. This is confirmed by the nucleation rate, which is high (Figure 6.9).

Next, we see that the mean particle radius (Figure 6.7) starts to increase. At the same time, the mean matrix concentration starts to fall and the particle volume fraction starts to rise rapidly. These effects are due to the growth phase of the particles; nearly all particles are growing since their radius is larger than the critical radius.

At $t \approx 2{\cdot}10^4$ the growth stops. As the material starts to attain its equilibrium composition, we notice multiple effects. The nucleation rate drops sharply, and the volume fraction as well as the matrix concentration start to stabilize. Additionally, the number of particles in the system starts to drop, and the mean and critical radius converge, but continue to increase. This is typical of the coarsening stage; the larger particles grow at the expense of the smaller ones, which are dissolving.

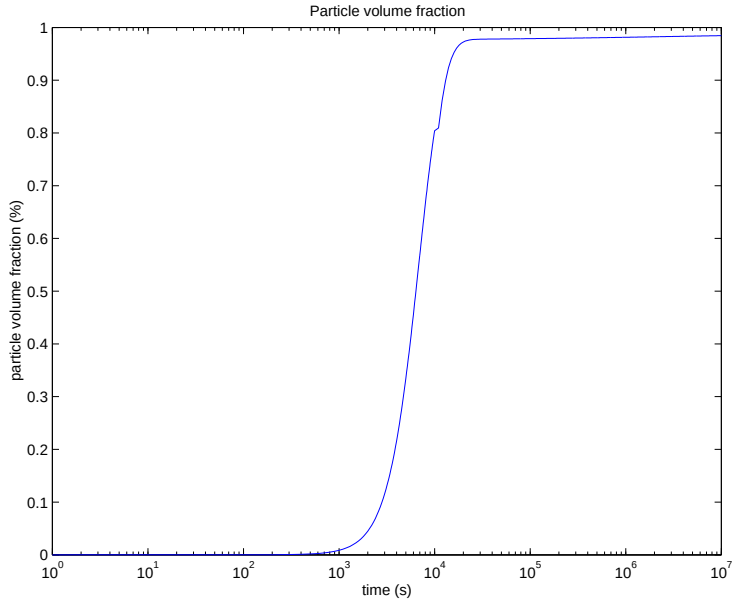

Figure 6.5: Particle volume fraction

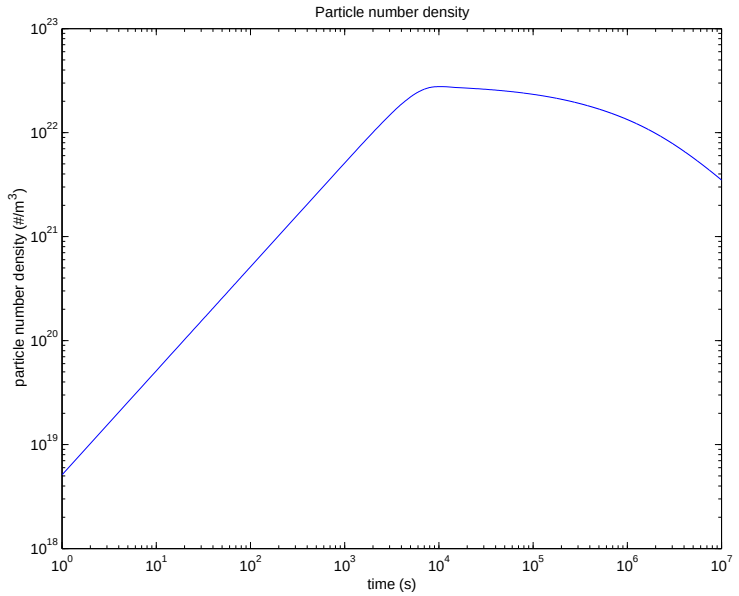

Figure 6.6: Particle number density

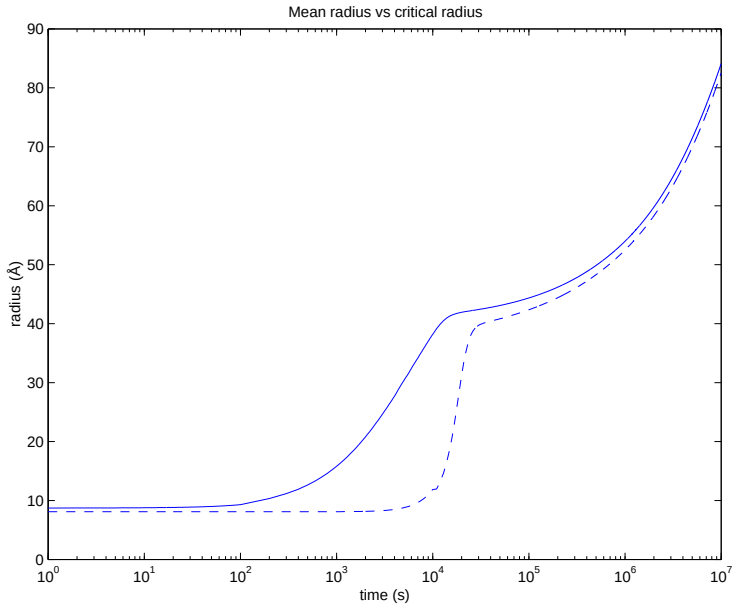

Figure 6.7: Mean radius (solid) and critical radius (dashed)

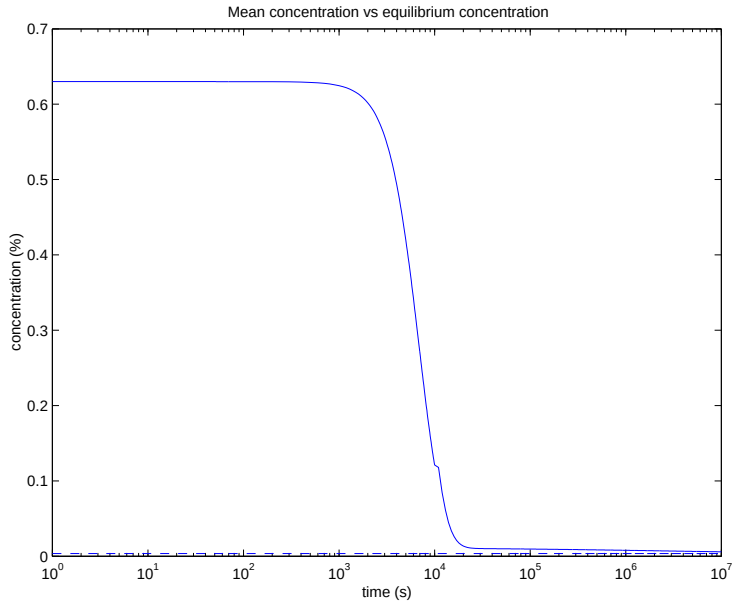

Figure 6.8: Matrix concentration (solid) and equilibrium concentration (dashed)

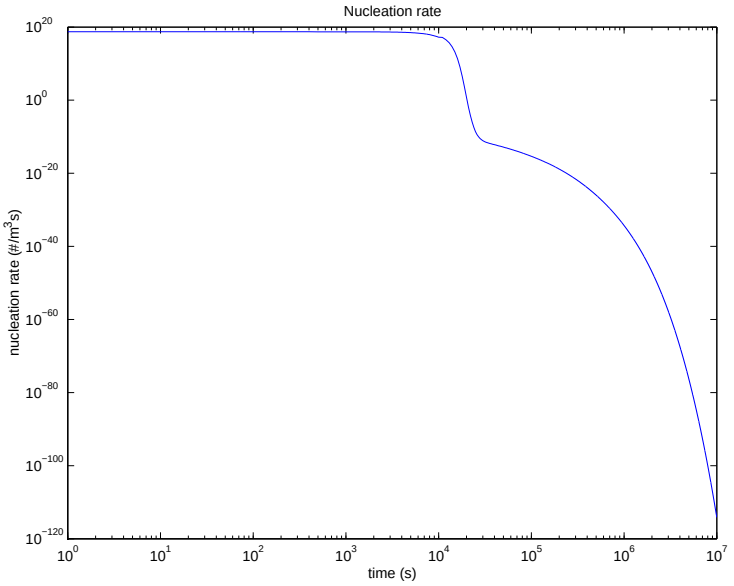

Figure 6.9: Nucleation rate

Chapter 7

Future work

Thusfar we have reviewed two separate models; one for the dissolution of the primary and secondary particles, and one for the nucleation of tertiary particles. The main goal of the project is to integrate these models to accommodate for both effects simultaneously. To accomplish this, a number of additional steps have to be taken:

- The nucleation model must be expanded to accommodate multi-component systems.
- The nucleation model must be embedded in the Stefan problem.
- A parameter study will need to be carried out to get a feeling for the way different parameters in the model influence the solutions.
- The resulting model will need to be tuned and validated with the use of data acquired through lab experiments.

7.1 Multi-component nucleation

In the current state, the nucleation model can only handle situations for binary systems. We will try to add multi-component support in the same way as we did for the Stefan problem. That means we will assume stoichiometry for the tertiary particles and demand that for each component the particle growth rate (as defined in Equation (3.11)) is equal in value, and the interface concentrations will have to satisfy an equation such as Equation (3.6). The situation is slightly more complicated because we need to take the Gibbs-Thomson effect into account as well.

7.2 Embedding the nucleation model

The integration of the models will be accomplished by adding a nucleation step to the dissolution algorithm:

1. Compute the concentration profiles solving the non-linear problem given by Equations (3.1)–(3.7),

2. Apply a step of the nucleation model for each volume of the Stefan problem. The size distribution for each volume will be stored and a correction will be applied to the concentrations in the Stefan problem volumes.
3. Predict the positions of S_1 and S_2 at the new time-step: $S_1(t + \Delta t)$ and $S_2(t + \Delta t)$, using Equation (3.7),
4. Redistribute the grid such that $S_1(t+\Delta t)$ and $S_2(t+\Delta t)$ are nodal points,
5. Return to step 1.

If sufficient time is still available, we may attempt to couple the two models more tightly.

7.3 Parameter study

In order to be able to tune the model intelligently, we need to have a good understanding of the interactions of the various parameters with the solutions. We hope to gain this insight by varying single parameters at a time and checking the way each change alters the solution.

7.4 Tuning and validating the model

Many of the required parameters (e.g. diffusion coefficients, solubility products) are not readily available. Experiments are necessary to determine the correct input values. After these values are obtained, we need to check if the model reproduces reality accurately.

Bibliography

William D. Callister, Jr. *Materials science and engineering : an introduction*. John Wiley & Sons, Inc., fifth edition, 1999. 6, 8, 10, 13

O.R. Myhr and Ø. Grong. Modelling of non-isothermal transformations in alloys containing a particle distribution. *Acta materiala*, 48:1605–1615, 2000. 16, 17, 25, 32

D.A. Porter and K.E. Easterling. *Phase transformations in metals and alloys*. Van Nostrand Reinhold (International) Co. Ltd., 1981. 6, 9, 10, 11

M.H. Protter and H.F. Weinberger. *Maximum principles in differential equations*. Prentice-Hall, Englewood Cliffs, 1967. 19

K.C. Russel. *Phase transformations*. A.S.M., 1970. 15

Fred Vermolen. *Mathematical Models for Particle Dissolution in Extrudable Aluminium Alloys*. PhD thesis, Delft University of Technology, 1998. 10, 18, 22, 29